PAPER

Optimising the materials for triboelectric nanogenerator to harvest the wrist pulse signal: a numerical study using the finite element method

V. Karthikeyan and S. Vivekanandan [ID] *

This study outlines the optimised materials used to improve the output performance of a triboelectric nanogenerator based on the contact separation mode. The selection of materials plays a crucial role in enhancing the output voltage of the triboelectric nanogenerator. This study involves the design of three distinct triboelectric nanogenerator models using polytetrafluoroethylene (PTFE), polydimethylsiloxane (PDMS), and silicone. Numerical analysis is conducted using the finite element method in COMSOL Multiphysics software to determine the output performance of these models under externally applied pulse pressure. The output voltage profiles of each model are compared, and it is observed that the PTFE-based model consistently produces an output voltage of 26 V when subjected to a pulse pressure of 3 kPa. These devices are well-suited for use in healthcare monitors, human motion detection, and gesture monitoring because of their inherent self-powering capability.

1. Introduction

Wearable sensors and self-powered biosensors are becoming increasingly necessary in the current developing society. Numerous energy-harvesting technologies, such as electromagnetic, piezoelectric, triboelectric, electrostatic, and pyroelectric technologies, are available to extract biological signals from the human body.[1] Of all these harvesting technologies, the triboelectric nanogenerator exhibits superior output performance compared to the others.[2] It is also easy to construct, uses a range of materials, and is self-powered, lightweight, inexpensive, reusable, and can be produced on a large scale.[3,4] Therefore, there has been an increasing focus on triboelectric nanogenerators (TENG). From a literature survey, it can be found that for wrist pulse acquisition, polymers are mostly used, especially polytetrafluoroethylene (PTFE), polydimethylsiloxane (PDMS), and silicone. PTFE is a fluorine-based polymer (fluoropolymer), with many industrial advantages. PTFE attracts electrons better than PDMS in the triboelectric series.[5] Research indicates that PTFE can produce charge densities of up to $\sim 5 \times 10^{-4}$ C m^{-2} for hundreds of years. PTFE's insulating properties sustain negative triboelectric charges for a long time. Contact mode structured PTFE-based TENGs generate more power and have the best electronegative properties under single mechanical pressure, with a charge affinity of 190 nC J^{-1}. PTFE-based TENGs offer outstanding mechanical qualities and substantial charge affinity differences, making them ideal for high power generation and output
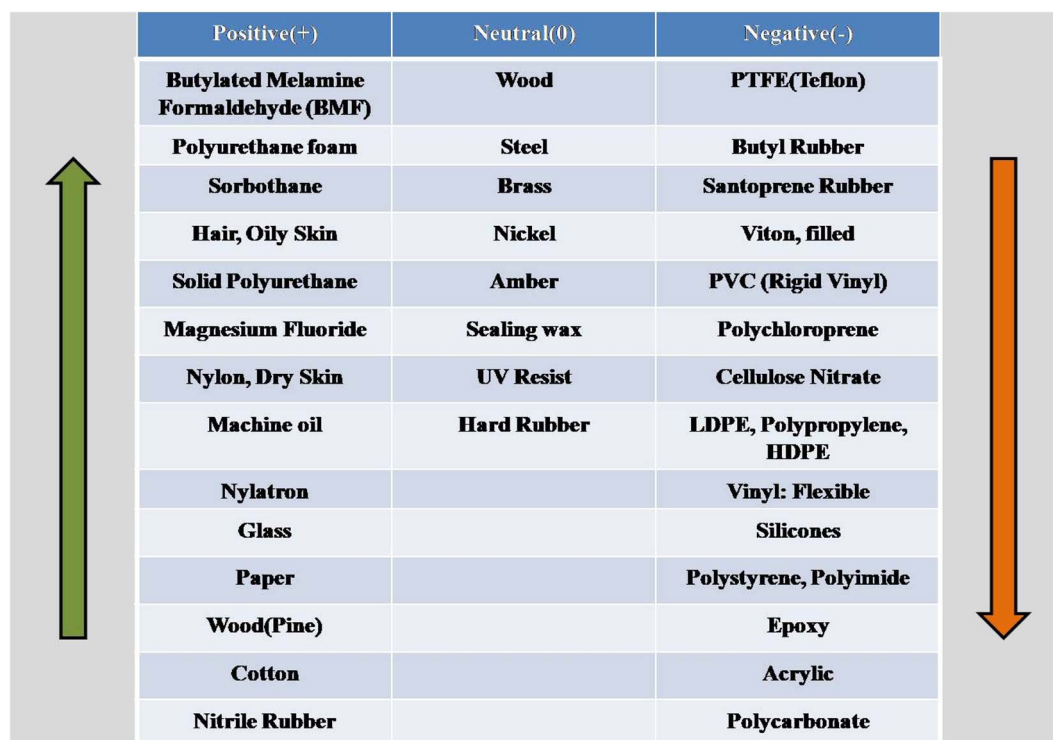
performance.[6] PDMS is a polymeric organsilicone chemical. Silicone connections with flexible polymer chains make it viscoelastic. Polydimethylsiloxane (PDMS) elastomers have been frequently employed in TENGs due to their outstanding triboelectric characteristics, flexibility, stretchability, and non-toxicity. By adding structures to the polymer's surface, its sensing capabilities can be modified.[7] Silicone is employed in triboelectric nanogenerators (TENGs) due to its chemical stability, flexibility, and advantageous position in the triboelectric series, which enables it to produce a substantial charge. A TENG's energy-harvesting and sensing capabilities can be improved by modifying silicone with additives, thereby rendering it suitable for applications such as wearable sensors and wave energy harvesting[8] Recent research shows that porous forms of the above polymers have better triboelectric characteristics than solid forms. Metallic/organic/inorganic materials have been employed to make porous polymer composites, which are better than solid ones.[9] A triboelectric nanogenerator (TENG) consists of two separate charged tribolayers. One layer can lose electrons, while the other layer can receive electrons when they come into contact or rub against each other. This phenomenon results in the generation of an electrical voltage between the electrodes of the triboelectric nanogenerator (TENG) by a combination of triboelectrification and electrostatic induction.[10] TENG operating modes can be categorised into four distinct types based on their operational characteristics. These modes include the single electrode mode, contact separation mode, lateral sliding mode, and free-standing mode. Among these modes, the contact separation mode is widely employed in various applications due to its superior output performance compared to the other modes.[11,12] Furthermore,

School of Electrical Engineering, Vellore Institute of Technology, Vellore, Tamil Nadu – 632 014, India. E-mail: svivekanandan@vit.ac.in

there are two methods by which the output performance of a TENG can be enhanced. By using a high-charge tribomaterial from the triboelectric series, the TENG can efficiently capture a small amount of mechanical energy.[13] Certain materials, such as wood, metal, silk, and polymers, exhibit an inherent triboelectrification effect.[14,15] Fig. 1 illustrates the wide range of material options available in the triboelectric series based on charge accumulation. John Carl Wilcke introduced the first triboelectric series for static charge in 1757.[16] By adding natural and synthetic polymers, the series can be extended to a certain extent with a similar order of some materials.[8] Various TENGs are constructed using different dielectric materials to capture wrist pulse pressure, and these are listed below. In 2018, Chen *et al.* designed a waterproof and stretchable triboelectric nanogenerator to harvest several types of biomechanical energy from the human body. The TENG carries a sandwiched micro-patterned frictional PDMS layer and stretchable electrode, and both are overlapped with a 2 mm air gap, and the entire structure is encapsulated by a stretchable PDMS layer. The thin and soft properties of stretchable PDMS allow the TENG to harvest mild vibrations like a wrist pulse, and the encapsulation protects the TENG from humidity changes.[17] Lin *et al.* in 2017 designed a self-powered, wireless, downy structured triboelectric nanogenerator (D-TENG). It carries two layers: one is a copper backing coated with surface-modified polytetrafluoroethylene (PTFE) films, and the other consists of plain copper thin films. Both layers are alternately attached to one end of an acrylic sheet, while their opposite ends are left free to move. Finally, the entire unit is encapsulated by stretchable rubber. Under low frequency operation, the fabricated D-TENG

produces electrical power of 2.28 mW with a conversion efficiency of 57.9% from human walking energy.[18] In 2018, Dong *et al.* introduced a stretchable and washable skin-inspired triboelectric nanogenerator (SI-TENG) for biomechanical and versatile pressure harvesting applications. The SI-TENG carries a base layer of a silicone rubber elastomer embedded with a zigzag interlaced silver-plated nylon yarn. The overall dimensions of the SI-TENG are 80×40 mm^2, and it produces an output voltage of 160 V. Therefore, the SI-TENG exhibits high sensitivity, fast detection and quick response as an energy harvester, as well in self-powered biosensors.[19] Another method, involving the introduction of the nanostructure on the tribolayer, can improve the generated output voltage.[20] The introduced nanostructure improves the frictional contact between the tribolayers, which ultimately improves the overall charge transfer between the tribolayers due to the generated voltage across the electrode of the TENG also being improved. The research on triboelectric nanogenerator surface modification is as follows.[21] S. M. Kim *et al.* in 2017 made a charge transfer comparison between a flat and structure-interfaced dielectric with metal TENGs. Here, aluminium serves as an electrode and polytetrafluoroethylene (PTFE) act as a dielectric layer, the top layer and the bottom dielectric layer are separated by an air gap with a thickness of 25 μm. To improve the output voltage of TENG, flat, cone, pyramid, circle and rectangular structures are introduced on its dielectric layer. From the above structured dielectric, the rectangular structured dielectric produces an improved transfer charge density; due to this the potential difference at the output terminal is high.[22] For effective harvesting of wrist pulse pressure in this work, both high-

Positive(+)	Neutral(0)	Negative(−)
Butylated Melamine Formaldehyde (BMF)	Wood	PTFE(Teflon)
Polyurethane foam	Steel	Butyl Rubber
Sorbothane	Brass	Santoprene Rubber
Hair, Oily Skin	Nickel	Viton, filled
Solid Polyurethane	Amber	PVC (Rigid Vinyl)
Magnesium Fluoride	Sealing wax	Polychloroprene
Nylon, Dry Skin	UV Resist	Cellulose Nitrate
Machine oil	Hard Rubber	LDPE, Polypropylene, HDPE
Nylatron		Vinyl: Flexible
Glass		Silicones
Paper		Polystyrene, Polyimide
Wood(Pine)		Epoxy
Cotton		Acrylic
Nitrile Rubber		Polycarbonate

Fig. 1   Triboelectric material series.

charge tribomaterials and rectangular surface morphology are used.

2. Sensor model

In this study, three distinct triboelectric nanogenerators are constructed using COMSOL Multiphysics software to capture wrist pulse pressure, as shown in Fig. 2. The designed TENGs function in contact separation mode. The contact separation modes are classified into two types: dielectric-to-dielectric mode and conductor-to-dielectric mode. As the conductor-to-dielectric mode gives an enhanced output performance, it is used in the suggested system.[12] In all of the modeled TENGs, the conductor is placed on top, serving as a tribolayer and an electrode, while the dielectric layer is positioned on the bottom, with its electrode connected back to the dielectric layer. An air gap is maintained between the conductor and the dielectric layer. The modeled TENG's dielectric layer, together with its electrode, is put on the location of the wrist pulse. The wrist pulse pressure has a magnitude of less than 3 kPa, causing deformation of the dielectric layer.[23] When pressure is present, this deformation causes the dielectric layer to come into contact with the top conductor; otherwise, the dielectric layer and the conductor separate. This contact separation operation creates charge transfers between the tribolayer and conductor; hence, the charge transfer density can be calculated using eqn (1):

$$\sigma' = \frac{\sigma x \varepsilon_{rp}}{t_1 \varepsilon_{rp} + t \varepsilon_{rp}} \tag{1}$$

where ε_{rp} is the polymer relative permittivity, t_1 is the polymer thickness, and x is an overlap interval. It resembles a capacitor, and the potential difference across the electrodes is given by eqn (2):

$$V = E_d + E_{air} x \tag{2}$$

$$E_d = -\frac{Q}{S \varepsilon_0 \varepsilon_r} \tag{3}$$

$$E_{air} = \frac{\sigma - \frac{Q}{S}}{\varepsilon_0} \tag{4}$$

$$E_{air} = \frac{Q}{S \varepsilon_0}\left[\frac{t_1}{\varepsilon_r} + x(t)\right]\frac{\sigma x(t)}{\varepsilon_0} \tag{5}$$

where E_d is the electric field of the polymer, given by eqn (3), and t_1 is the thickness of the polymer. E_{air}, the electric field in the air gap, is obtained using eqn (4) and (5). x is the air gap interval, S is the metal area, ε_0 is the permittivity of a vacuum, ε_r is the relative dielectric constant, and σ is the inner surface

tribocharge. The open circuit voltage is then given below in eqn (6):

$$V_{OC} = \frac{\sigma x(t)}{\varepsilon_0} \tag{6}$$

The potential difference under short circuit conditions is zero, so the overall charge transferred (Q) is obtained using eqn (7):

$$Q = \frac{S\sigma(t)\varepsilon_r}{t_1 + x(t)\varepsilon_r} \tag{7}$$

The generated load current is obtained using eqn (8):

$$I = C\frac{dV}{dt} + V\frac{dC}{dt} \tag{8}$$

where C is the capacitance, and V is the voltage across the electrodes.

3. Design of triboelectric nanogenerators

This study presents the design of three distinct triboelectric nanogenerators (TENGs) utilising three different topmost negative tribomaterials, namely PDMS, silicone, and PTFE, for the purpose of measuring wrist pulse pressure. Copper is employed as the positive layer and serves as the top electrode in each triboelectric nanogenerator (TENG), while aluminium is utilised as the negative electrode for all TENGs, which is securely attached to the negative tribolayers. All of the produced triboelectric nanogenerator (TENG) models exhibit circular shapes with identical dimensions. This is due to the fact that the circular shape of TENGs allows for uniform deformation when subjected to external pulse pressure.[24] The positive tribolayer of the designed TENGs has a diameter of 1 μm and a thickness of 0.2 μm. Subsequently, each negative tribolayer has a diameter of 1 μm and a thickness of 0.18 μm. Finally, the negative electrode has a thickness of 0.02 μm. Positive and negative tribolayers are positioned at 0.07 μm intervals from each other. By introducing the rectangular surface morphology, which improves the frictional contacts between the tribolayers, the output performance of the designed TENGs can be enhanced. As a result, a rectangular nanostructure with the following dimensions is formed on the top surface of the negative tribolayer: 0.08 μm in width, 0.08 μm in depth, and 0.08 μm in height. The array feature in the COMSOL Multiphysics software is utilised to populate the rectangular structure across the full surface negative tribolayer. Subsequently, the
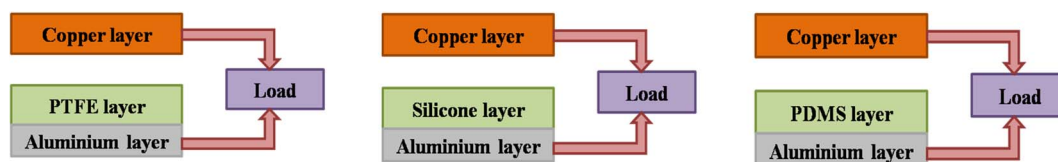

Fig. 2 Models of three different triboelectric nanogenerators for wrist pulse acquisition.

nanostructures can be merged with the negative tribolayer using the union operation. However, the positive layer lacks any nanostructure and is characterised by a plain and smooth surface. Once the structural design and material selection have been finalised, the physics component must be chosen from the physics option inside the COMSOL Multiphysics software, as determined during the study. A solid mechanical interface is initially employed to simulate the modelled TENGs from the perspective of structural mechanics. This interface translates the externally provided wrist pulse pressure into displacement. The displacement facilitates contact between the tribolayers, leading to a charge transfer process. The rate of charge transfer is contingent upon the displacement, which in turn is influenced by the pulse pressure. In the absence of pulse pressure, the tribolayers do not experience any movement throughout the interval separation process. A potential difference across the electrode will be generated during the separation process due to the transfer of charge from the contact action. An induced voltage between the electrodes of the simulated TENGs is obtained *via* the electrostatic interface from the AC/DC. Finally, meshing is employed to shorten the modeled TENGs' simulation time. Meshing divides the TENG structure into discrete parts, each of which is then simulated, resulting in a reduction in the total simulation time. The simulated output response of the planned TENG is observed using a stationary study. The

aforementioned steps are crucial for simulating any model in COMSOL Multiphysics.

4. Results and discussion

The mechanical analysis in this section determines the range of deformation produced by the three distinct TENGs in response to a specified external pulse pressure. The electrical analysis provides the open circuit output voltage generated by the three TENGs in response to the same deformation.

4.1 Solid mechanics

The solid mechanical interface in COMSOL Multiphysics software is well-suited for structural analysis. Its performance is based on Navier's equation. Stress *versus* strain analysis is a commonly employed method.[25] Three distinct triboelectric nanogenerators (TENGs) have been designed in three dimensions, as depicted in Fig. 3(A–C). The dimensions of these TENGs are provided in the preceding section. The negative electrode of the modelled triboelectric nanogenerators (TENGs) is positioned at the site of wrist pulse pressure in order to collect wrist pulse pressure data for the purpose of blood pressure detection.[26] Blood pressure is mostly attributed to irregularities of the *vata nadi* (cun).[27] Consequently, the *vata nadi* is employed in this context for the purpose of blood pressure detection. The
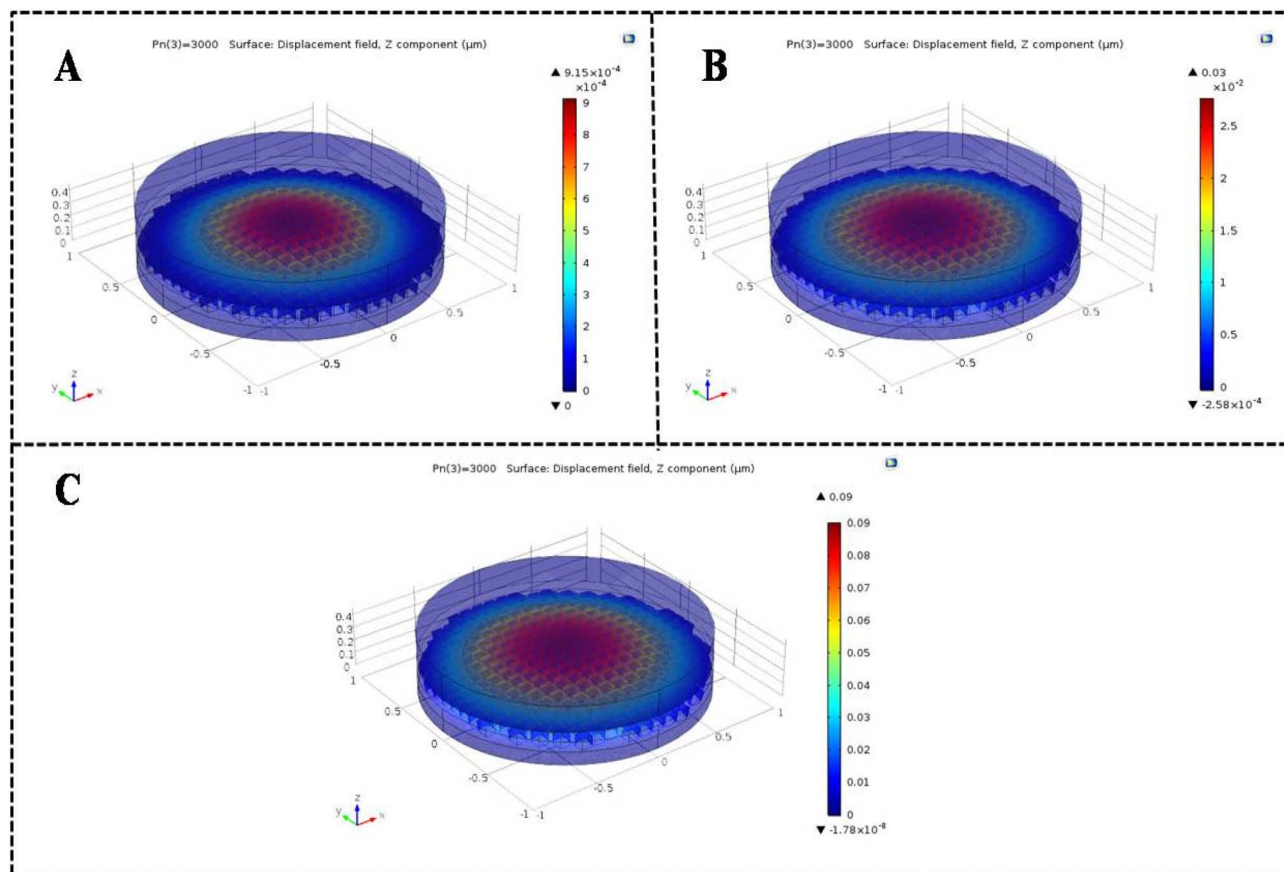

Fig. 3 Three different triboelectric nanogenerator models: structural view and output displacement for 3 kPa of input pulse pressure. (A) PTFE-based TENG. (B) Silicone-based TENG. (C) PDMS-based TENG.

Table 1 Output displacement of three different TENGs for 0–3 kPa of input pulse pressure
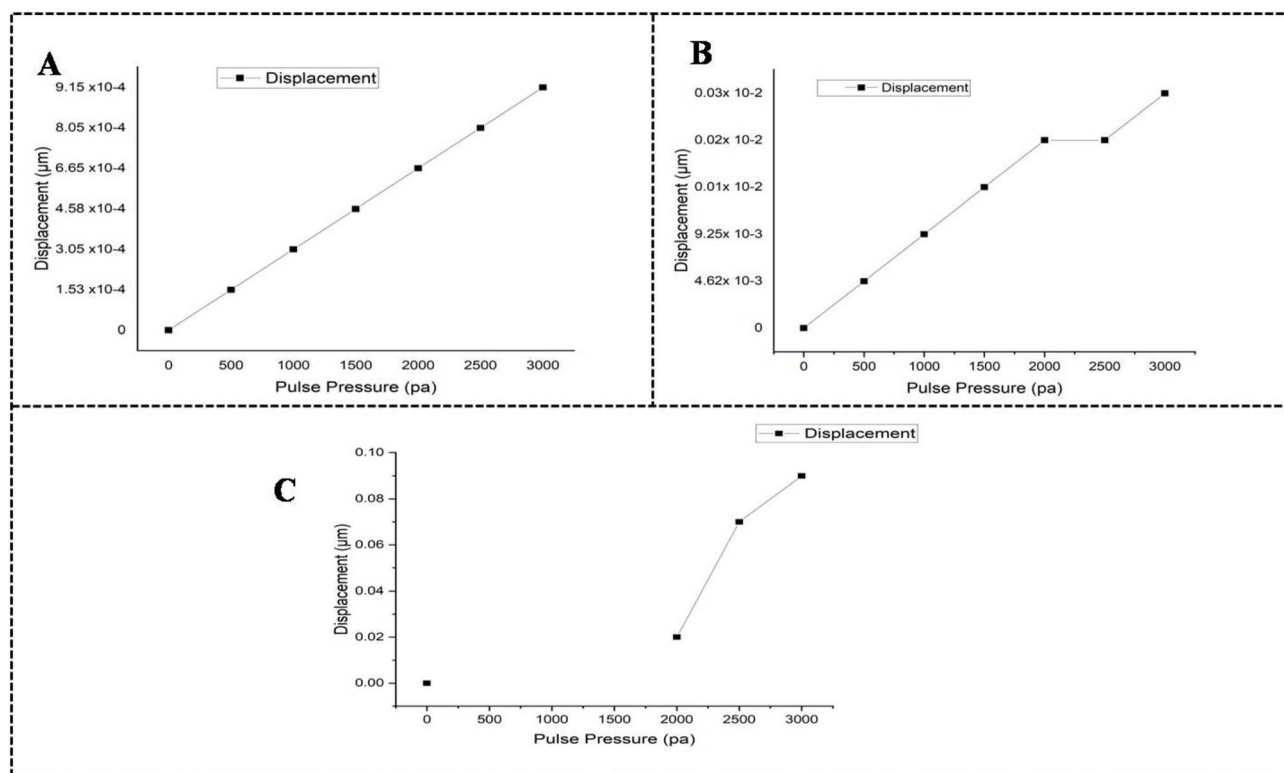
S. no.	Pulse pressure (Pa)	PTFE-based TENG (µm)	Silicone-based TENG (µm)	PDMS-based TENG (µm)
1	0	0	0	0
2	500	1.53×10^{-4}	4.62×10^{-3}	0.03×10^{-2}
3	1000	3.05×10^{-4}	9.25×10^{-3}	0.04×10^{-2}
4	1500	4.58×10^{-4}	0.01×10^{-2}	0.05×10^{-2}
5	2000	6.65×10^{-4}	0.02×10^{-2}	0.02
6	2500	8.05×10^{-4}	0.02×10^{-2}	0.07
7	3000	9.15×10^{-4}	0.03×10^{-2}	0.09

vata nadi exhibits a pressure range that falls within the range of wrist pulse pressure. Therefore, to simulate the three separate triboelectric nanogenerators (TENGs) being studied, wrist pulse pressure is employed. The input parameter in this interface is derived from the wrist pulse, which exhibits pressure within a range of less than 3 kPa. For 3 kPa of input pulse pressure, the negative layer of the PTFE-based TENG is displaced in the range of 9.15×10^{-4} µm, and similarly, the displacements of the negative layers of silicone-based and PDMS-based TENGs are in the range of 0.03×10^{-2} and 0.09 µm, respectively. The displacements of the negative layers of three distinct TENGs under externally applied pulse pressure ranging from 0 to 3000 Pa are shown in Table 1. The parameters of displacement *versus* pulse pressure are shown in Fig. 4(A–C). In contrast to the other TENGs, Fig. 4(A) demonstrates that the PTFE-based TENG exhibits a linear relationship between the applied pulse pressure and output displacement. Furthermore, the displacement only controls the total charge transfer between the two tribolayers that face each other. Therefore, PTFE is a good material for designing a TENG in order to harvest wrist pulse pressure. A fixed constraint option in the solid mechanical interface allows the modelled TENGs to have their circumference maintained continuously while they are being simulated. This keeps the TENG stable when applying pulse pressure. The modelled TENG is subjected to pulse pressure through the usage of the boundary load option in this interface. Furthermore, this interface uses normal meshing, which responds quickly when simulating the modelled TENGs. This interface uses stationary studies to show the simulated output response.

4.2 Electrostatics

By utilising this interface, one can examine the output potential difference of any given model. The displacement is provided to the simulated TENG, which subsequently transforms it into voltage. In this interface, the output displacement obtained in the previous interface of three different modelled TENGs is used to maintain the gap between the positive and negative tribolayers of the modelled TENGs. For the PTFE-based TENG, the separation gap between the tribolayers is 9.15×10^{-4} µm, for the PDMS-based TENG, the separation gap between the tribolayers is maintained at 0.09 µm, and finally for the silicone-based TENG, the separation gap between the tribolayers is maintained at 0.03×10^{-2} µm. The output voltage between the

Fig. 4 Input pulse pressure *versus* output displacement of three different TENGs. (A) PTFE-based TENG. (B) Silicone-based TENG. (C) PDMS-based TENG.
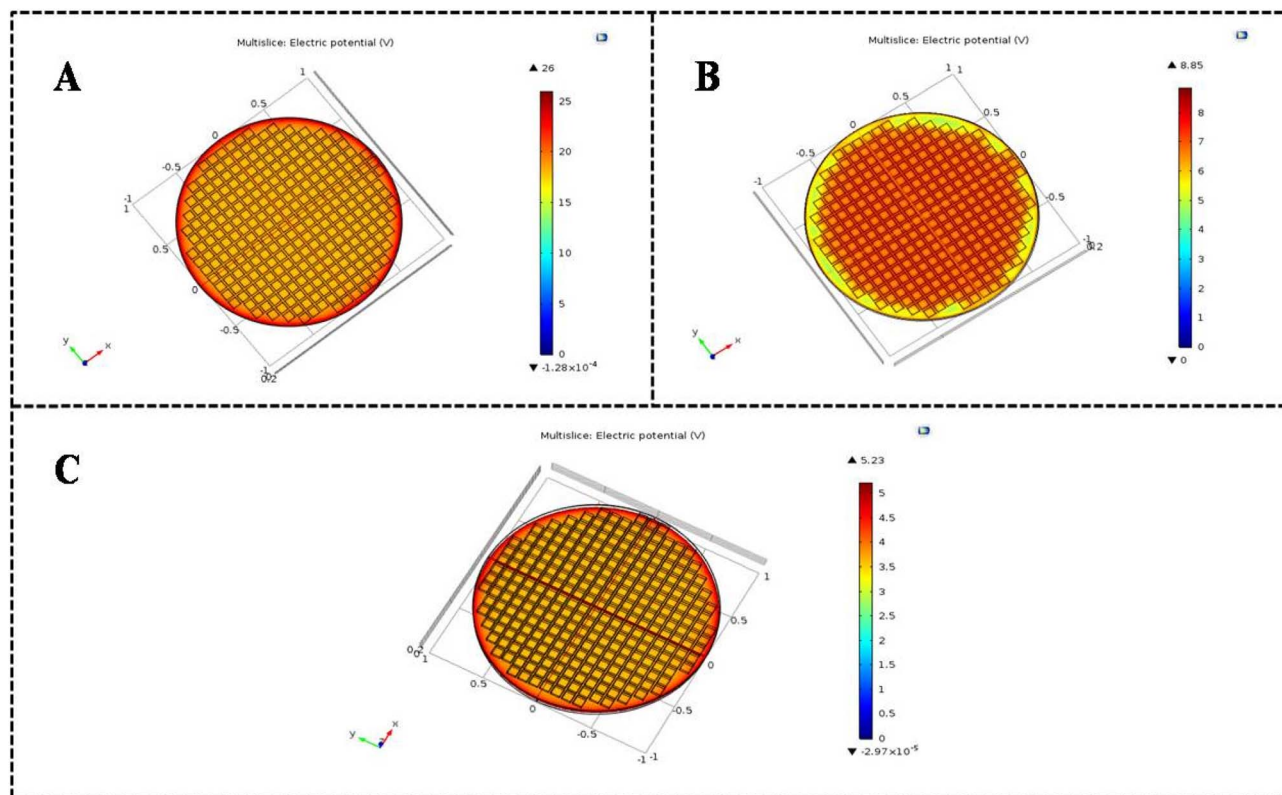
Fig. 5 Three different triboelectric nanogenerator models: structural views and induced output voltages. (A) PTFE-based TENG. (B) Silicone-based TENG. (C) PDMS-based TENG.

Table 2 Surface charge density values for positive and three different negative layers

S. no.	Material	Surface charge density value ($\mu C\ m^{-2}$)
1	Polytetrafluoroethylene (PTFE)	8×10^{-6}
2	Polydimethylsiloxane (PDMS)	54.49
3	Silicone	100
4	Copper	5×10^{-4}

electrodes of the simulated TENGs is determined by the gap between the tribolayers. The presence of pulse pressure facilitates the interaction between the negative tribolayer and the positive tribolayer, resulting in a charge transfer between the two tribolayers. In the absence of pulse pressure, the tribolayers undergo separation, resulting in the transfer of charge and subsequent generation of a voltage across the electrodes of the modelled triboelectric nanogenerator (TENG). The structural views and induced potential differences of the three distinct modelled triboelectric nanogenerators (TENGs) are depicted in Fig. 5(A–C). In order to observe the induced potential difference, it is necessary to provide grounding for any of the electrodes. In this case, the bottom electrode is grounded by utilising the ground option within the interface. Furthermore, the float potential within this interface is employed to determine the potential difference between the electrode and the ground terminal. The tribolayer surface charge densities are given as

Table 3 Output voltages of three different TENGs for given input displacements

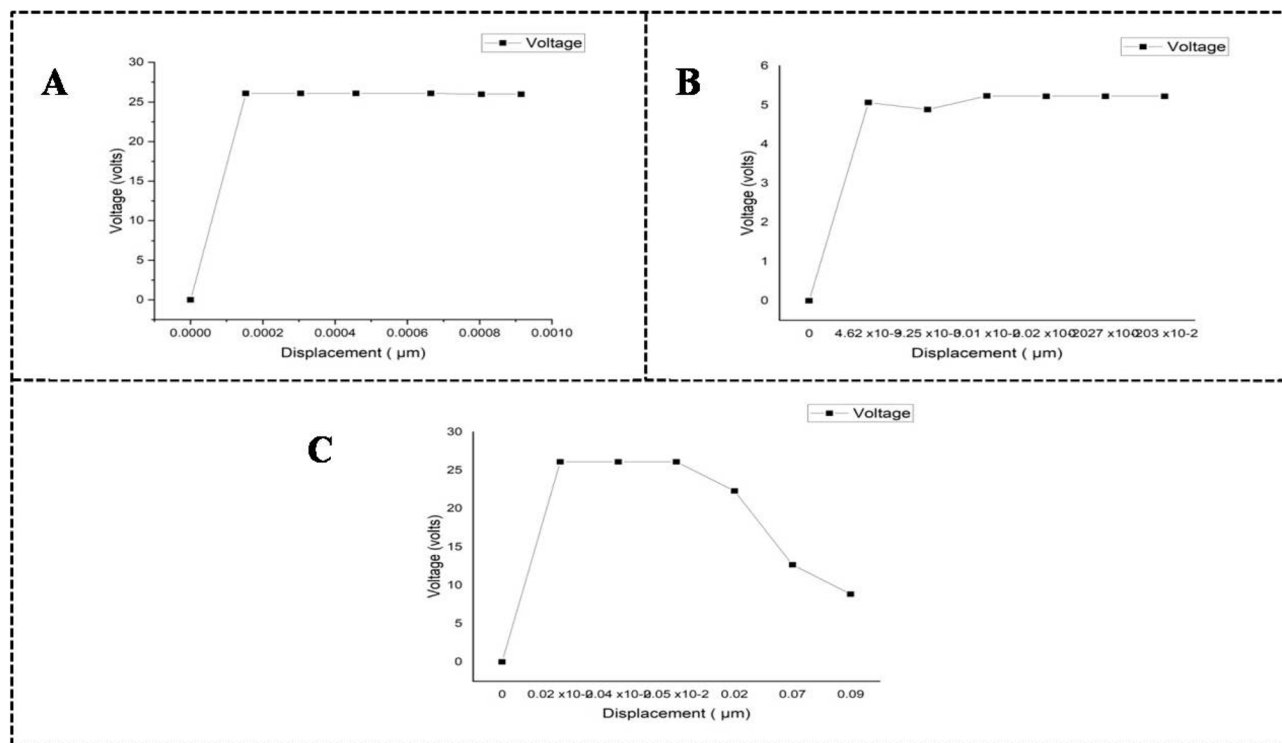| S. no.	PTFE-based TENG		Silicone-based TENG		PDMS-based TENG	
	Input displacement (μm)	Output voltage (V)	Input displacement (μm)	Output voltage (V)	Input displacement (μm)	Output voltage (V)
1	0	0	0	0	0	0
2	1.53×10^{-4}	26.1	4.62×10^{-3}	5.07	0.02×10^{-2}	26.1
3	3.05×10^{-4}	26.1	9.25×10^{-3}	4.89	0.04×10^{-2}	26.1
4	4.58×10^{-4}	26.1	0.01×10^{-2}	5.24	0.05×10^{-2}	26.1
5	6.65×10^{-4}	26.1	0.02×10^{-2}	5.23	0.02	22.3
6	8.05×10^{-4}	26	0.027×10^{-2}	5.23	0.07	12.7
7	9.15×10^{-4}	26	0.03×10^{-2}	5.23	0.09	8.85

Fig. 6 Input displacement *versus* output voltage for three different TENGs. (A) PTFE-based TENG. (B) Silicone-based TENG. (C) PDMS-based TENG.

per the values in Table 2. In this interface, coarse meshing is employed to simulate the modelled TENGs, resulting in a shorter simulation time. A stationary study is employed after simulating the modelled triboelectric nanogenerators (TENGs) to investigate the output response. The induced output voltages of the three distinct modelled TENGs in response to an externally supplied input displacement are presented in Table 3. The output characteristics in terms of the relationships between the induced voltage and displacement are illustrated in Fig. 6(A–C). Fig. 6(A) shows that the output curve of the PTFE-based TENG exhibits a linear relationship until a specific displacement is reached, after which the output remains stable as the displacement increases. In contrast, the curve of the PDMS-based TENG shows that the output increases linearly and then decreases as the displacement increases. However, the silicone-based TENG generates a low output voltage, which poses a challenge in activating subsequent measuring units. It can be inferred that the PTFE-based TENG is the preferred option for acquiring wrist pulse pressure.

5. Conclusion

Three distinct TENGs are designed and simulated using the COMSOL Multiphysics software to detect blood pressure. The displacements and induced output open circuit voltages of three distinct modelled TENGs are determined using the finite element method. Among the three different TENGs, the PTFE-based TENG produces an improved output performance for an externally applied input pulse pressure. Hence, PTFE is an

optimised material in the design of TENGs for detecting blood pressure. The sizes of the created TENGs allow them to harvest the biological signal. The designed TENGs have the capacity to effectively harvest a variety of biological information, including motion, breathing rate, heart rate, and gesture monitoring.

Ethical statement

No humans were involved in this research.

Author contributions

Karthikeyan V.: conceived and designed the experiments; performed the experiments; analyzed and interpreted the data; contributed reagents, materials, analysis tools or data; wrote the paper. Vivekanandan S.: conceived and designed the experiments; analyzed and interpreted the data; contributed reagents, materials, analysis tools or data.

Conflicts of interest

On behalf of all authors, the corresponding author states that there is no conflict of interest.

Data availability

The triboelectric nanogenerator (TENG) was designed and analyzed using COMSOL Multiphysics software. All design steps

and relevant dimensions are detailed in the TENG design section of the manuscript.

References

1 T. Quan, X. Wang, Z. L. Wang and Y. Yang, Hybridized Electromagnetic-Triboelectric Nanogenerator for a Self-Powered Electronic Watch, *ACS Nano*, 2015, **9**(12), 12301–12310, DOI: **10.1021/acsnano.5b05598**.

2 B. Xie, *et al.*, Advances in Graphene-Based Electrode for Triboelectric Nanogenerator, *Nano-Micro Lett.*, 2025, **17**(1), 17, DOI: **10.1007/s40820-024-01530-1**.

3 Q. Shi, T. He and C. Lee, More than energy harvesting – Combining triboelectric nanogenerator and flexible electronics technology for enabling novel micro-/nano-systems, *Nano Energy*, 2019, **57**(October 2018), 851–871, DOI: **10.1016/j.nanoen.2019.01.002**.

4 K. Venugopal, P. Panchatcharam, A. Chandrasekhar and V. Shanmugasundaram, Comprehensive Review on Triboelectric Nanogenerator Based Wrist Pulse Measurement: Sensor Fabrication and Diagnosis of Arterial, *Pressure*, 2021, **6**(5), 1681–1694, DOI: **10.1021/acssensors.0c02324**.

5 Y. Yang, *et al.*, Single-electrode-based sliding triboelectric nanogenerator for self-powered displacement vector sensor system, *ACS Nano*, 2013, **7**(8), 7342–7351, DOI: **10.1021/nn403021m**.

6 X. Cui, *et al.*, Pulse sensor based on single-electrode triboelectric nanogenerator, *Sens. Actuators, A*, 2018, **280**, 326–331, DOI: **10.1016/j.sna.2018.07.051**.

7 M. Muthu, R. Pandey, X. Wang, A. Chandrasekhar, I. A. Palani and V. Singh, Enhancement of triboelectric nanogenerator output performance by laser 3D-Surface pattern method for energy harvesting application, *Nano Energy*, 2020, **78**, 105205, DOI: **10.1016/j.nanoen.2020.105205**.

8 Y. C. Lai, J. Deng, S. L. Zhang, S. Niu, H. Guo and Z. L. Wang, Single-Thread-Based Wearable and Highly Stretchable Triboelectric Nanogenerators and Their Applications in Cloth-Based Self-Powered Human-Interactive and Biomedical Sensing, *Adv. Funct. Mater.*, 2017, **27**(1), 1–10, DOI: **10.1002/adfm.201604462**.

9 M. Mariello, Novel Flexible Triboelectric Nanogenerator based on Metallized Porous PDMS and Parylene C, *Energies*, 2020, 1–12.

10 K. Meng, *et al.*, Flexible Weaving Constructed Self-Powered Pressure Sensor Enabling Continuous Diagnosis of Cardiovascular Disease and Measurement of Cuffless Blood Pressure, *Adv. Funct. Mater.*, 2019, **29**(5), 1–10, DOI: **10.1002/adfm.201806388**.

11 C. Wu, A. C. Wang, W. Ding, H. Guo and Z. L. Wang, Triboelectric Nanogenerator: A Foundation of the Energy for the New Era, *Adv. Energy Mater.*, 2019, **9**(1), 1–25, DOI: **10.1002/aenm.201802906**.

12 H. Chen, Y. Xu, J. Zhang, W. Wu and G. Song, Theoretical System of Contact-Mode Triboelectric Nanogenerators for High Energy Conversion Efficiency, *Nanoscale Res. Lett.*, 2018, 346.

13 J. H. Lee, *et al.*, Control of Skin Potential by Triboelectrification with Ferroelectric Polymers, *Adv. Mater.*, 2015, **27**(37), 5553–5558, DOI: **10.1002/adma.201502463**.

14 J. K. Mainra, A. Kaur, G. Sapra and P. Gaur, Simulation and Modelling of Triboelectric Nanogenerator for Self-powered Electronic Devices, *IOP Conf. Ser.:Mater. Sci. Eng.*, 2022, **1225**(1), 012012, DOI: **10.1088/1757-899x/1225/1/012012**.

15 X. Zhang, *et al.*, Bioinspired Flexible Kevlar/Hydrogel Composites with Antipuncture and Strain-Sensing Properties for Personal Protective Equipment, *ACS Appl. Mater. Interfaces*, 2024, **16**(34), 45473–45486, DOI: **10.1021/acsami.4c08659**.

16 J. W. Lee, B. U. Ye and J. M. Baik, Research Update: Recent progress in the development of effective dielectrics for high-output triboelectric nanogenerator, *APL Mater.*, 2017, **5**(7), 073802, DOI: **10.1063/1.4979306**.

17 X. Chen, *et al.*, Waterproof and stretchable triboelectric nanogenerator for biomechanical energy harvesting and self-powered sensing, *Appl. Phys. Lett.*, 2018, **112**(20), 1–6, DOI: **10.1063/1.5028478**.

18 Z. Lin, *et al.*, Triboelectric Nanogenerator Enabled Body Sensor Network for Self-Powered Human Heart-Rate Monitoring, *ACS Nano*, 2017, **11**(9), 8830–8837, DOI: **10.1021/acsnano.7b02975**.

19 K. Dong, *et al.*, A Stretchable Yarn Embedded Triboelectric Nanogenerator as Electronic Skin for Biomechanical Energy Harvesting and Multifunctional Pressure Sensing, *Adv. Mater.*, 2018, **30**(43), 1–12, DOI: **10.1002/adma.201804944**.

20 N. Ma, *et al.*, Enhancing the sensitivity of spin-exchange relaxation-free magnetometers using phase-modulated pump light with external Gaussian noise, *Opt. Express*, 2024, **32**(19), 33378, DOI: **10.1364/oe.530764**.

21 P. Bai, *et al.*, Membrane-Based Self-Powered Triboelectric Sensors for Pressure Change Detection and Its Uses in Security Surveillance and Healthcare Monitoring, *Adv. Funct. Mater.*, 2014, **24**(37), 5807–5813, DOI: **10.1002/adfm.201401267**.

22 S. M. Kim, J. Ha and J. B. Kim, Morphology effect on the transferred charges in triboelectric nanogenerators: Numerical study using a finite element method, *Integr. Ferroelectr.*, 2017, **183**(1), 19–25, DOI: **10.1080/10584587.2017.1375820**.

23 Y. Shu, C. Li, Z. Wang, W. Mi, Y. Li and T. Ren, A Pressure Sensing System for Heart Rate Monitoring with Polymer-Based Pressure Sensors and an Anti-Interference Post Processing Circuit, *Sensors*, 2015, 3224–3235, DOI: **10.3390/s150203224**.

24 A. A. Mathew and S. Vivekanandan, Design and Simulation of Single-Electrode Mode Triboelectric Nanogenerator-Based Pulse Sensor for Healthcare Applications Using COMSOL Multiphysics, *Energy Technol.*, 2022, **2101130**, 1–12, DOI: **10.1002/ente.202101130**.

25 X. Zhang, Y. Liu, X. Chen, Z. Li and C. Y. Su, Adaptive Pseudoinverse Control for Constrained Hysteretic Nonlinear Systems and its Application on Dielectric Elastomer Actuator, *IEEE/ASME Trans. Mechatronics*, 2023, **28**(4), 2142–2154, DOI: **10.1109/TMECH.2022.3231263**.

26 K. Venugopal and V. Shanmugasundaram, Effective Modeling and Numerical Simulation of Triboelectric Nanogenerator for Blood Pressure Measurement Based on Wrist Pulse Signal Using Comsol Multiphysics Software, *ACS Omega*, 2022, **7**(30), 26863–26870, DOI: **10.1021/acsomega.2c03281**.

27 M. Menon and A. Shukla, Journal of Ayurveda and Integrative Medicine Understanding hypertension in the light of Ayurveda, *J. Ayurveda Integr. Med.*, 2017, 1–6, DOI: **10.1016/j.jaim.2017.10.004**.